

Local integrals of motion encoded in a few eigenstates

J. Pawłowski,¹ P. Łydzba,¹ and M. Mierzejewski¹

¹*Institute of Theoretical Physics, Faculty of Fundamental Problems of Technology,
Wrocław University of Science and Technology, 50-370 Wrocław, Poland*

Many properties of a quantum system can be obtained from just a single eigenstate of its Hamiltonian. For example, a single eigenstate can be used to determine whether a system is integrable or chaotic and, in the latter case, to establish its thermal properties. Focusing on the XXZ model, we show that the local integrals of motion, which lie at the heart of integrability, can also be estimated from a small number of eigenstates. Moreover, as the system size increases, fewer eigenstates are required, so that in the thermodynamic limit, the integrals of motion can be obtained from a vanishingly small fraction of all eigenstates. Interestingly, this property does not extend to integrals of motion arising solely from Hilbert space fragmentation, as found in the folded XXZ model, where the majority of eigenstates has to be used. This represents one of the few fundamental differences known between integrability and Hilbert space fragmentation.

I. INTRODUCTION

Over the past two decades, significant effort has been devoted to understanding the non-equilibrium dynamics of closed quantum systems [1–4]. In particular, whether and, if yes, why the expectation values of local observables at long times agree with the predictions of standard Gibbs ensembles. This behavior is known as thermalization, while systems that exhibit it are commonly referred to as ergodic.

These studies have shown that a great deal of information can be extracted from just a single eigenstate in the thermodynamic limit, or from a small number of eigenstates in a finite system [5]. For example, it can be used to identify ergodic behavior. The bipartite entanglement entropy of a single eigenstate, which quantifies correlations between subsystems, is universal in ergodic systems. Specifically, its leading term matches that of a random state from the Hilbert space [6] and is maximal in the thermodynamic limit [7–11]. The only restriction is that the eigenstate cannot be too close to the edges of the spectrum [12]. For this reason, it has been used in studies of ergodicity-breaking transitions to pinpoint the transition point [13–17].

Moreover, thermalization is currently understood through the Eigenstate Thermalization Hypothesis (ETH), which asserts that individual eigenstates are essentially thermal [18–20]. This means that the expectation values of local observables in a single eigenstate agree with the predictions of standard Gibbs ensembles. Consequently, a single eigenstate is not only sufficient to identify ergodicity, but also encodes the equilibrium properties of ergodic systems.

The most studied exceptions to thermalization are integrable models. Here, we focus on a paradigmatic example, the XXZ spin chain [21–23]. Integrable models support an extensive number of local integrals of motion (LIOMs), which are local operators that commute with the Hamiltonian, ensuring that their expectation values are conserved during time evolution. Integrable models do not satisfy the ETH, so their eigenstates are not ther-

mal [24–27]. Nevertheless, in this work, we demonstrate that a small number of eigenstates suffices to determine LIOMs and, in principle, to construct the Generalized Gibbs Ensemble [28–34]. Importantly, this number does not increase with system size, meaning that it represents a vanishing fraction of the Hilbert space dimension. This leads to the surprising conclusion that a small number of eigenstates can provide an accurate description of the stationary state also in an integrable model. The identification of LIOMs also provides the starting point for constructing hydrodynamics or generalized hydrodynamics [35–46].

Finally, we verify whether this observation holds in systems exhibiting Hilbert space fragmentation [47–54]. In this ergodicity-breaking phenomenon, the Hamiltonian, when written in a suitable local basis, decomposes into exponentially many disconnected blocks. Each block contains an exponentially small fraction of all eigenstates. This phenomenon is also believed to be distinct from integrability. Although some fragmented systems are known to support LIOMs [55], it remains unclear whether all do. Furthermore, a seminal work connected Hilbert space fragmentation to a different class of conserved operators, which are not strictly local but behave as local in typical states from the Hilbert space [56, 57]. Despite this, there are not many reported differences between integrability and Hilbert space fragmentation.

For this reason, we focus on the folded XXZ model, which can be obtained from the XXZ model in the limit of infinite anisotropy [58–60]. We demonstrate that, apart from LIOMs stemming from Bethe-ansatz integrability (which vanish when a perturbation breaking Bethe-ansatz integrability is introduced), the model also hosts LIOMs originating from fragmentation (which do not vanish under such perturbations). We observe that the former can still be numerically generated from a small number of eigenstates, while the latter require almost all eigenstates. This leads to the conclusion that the information about LIOMs originating from fragmentation is encoded differently in eigenstates.

The paper is organized as follows. In Sec. II, we introduce the numerical method used to estimate LIOMs from

an incomplete set of eigenstates. In Sec. III, we demonstrate that this estimation is accurate for a small number of eigenstates in the XXZ spin chain. We consider different symmetry sectors and extend our study to quasilocal integrals of motion. In Sec. IV, we examine the effectiveness of the estimation in the folded XXZ model. Finally, we summarize our findings and conclude in Sec. V.

II. FINDING LIOMS FROM INCOMPLETE SPECTRUM

We first discuss the numerical method for estimating LIOMs, denoted hereafter as \hat{Q}^α , from an incomplete set of eigenstates of the Hamiltonian, $H|n\rangle = E_n|n\rangle$. Here, the index α labels LIOMs. We focus on Hermitian operators, for which we use the Hilbert-Schmidt (HS) product $\langle AB \rangle = \text{Tr}(AB)/Z$ and the HS norm $\|A\|^2 = \langle AA \rangle$, where the trace is calculated over the *entire* Hilbert space with dimension Z . We require that $\|A\|^2 = 1$. For simplicity, we first consider a nondegenerate spectrum. This assumption is not essential, and minor modifications allow to study systems with degenerate eigenvalues. This is discussed in sections III and IV. Note that, in a case of nondegenerate spectrum, conserved quantities have nonvanishing matrix elements only along the diagonal, i.e., $\langle m|\hat{Q}^\alpha|n\rangle \neq 0$ only for $m = n$. Therefore, in order to confirm that \hat{Q}_α is conserved, one needs to calculate at least all diagonal matrix elements and verify that $1/Z \sum_n \langle n|\hat{Q}^\alpha|n\rangle^2 = \|\hat{Q}^\alpha\|^2$. This task requires full diagonalization of the Hamiltonian, posing a bottleneck for numerical studies.

In order to estimate LIOMs from selected eigenstates, it is necessary to implement a method that does not rely on the HS product or HS norm (unlike the one employed in [61–63]). An appropriate approach has recently been introduced in Ref. [55]. It is based on the observation that LIOMs can be obtained from compressing the information stored in the diagonal matrix elements of local operators, $A_{nn}^s = \langle n|\hat{A}^s|n\rangle$. By local operators, we mean (sums of) operators that act nontrivially on a finite subvolume of a system in the thermodynamic limit. To this end, we consider a set of D_O orthonormal local operators $\{A^1, \dots, A^{D_O}\}$, which satisfy $\langle A^i A^j \rangle = \delta_{ij}$. Next, we construct a matrix of dimension $Z \times D_O$ composed of their diagonal matrix elements,

$$\mathcal{R} = \begin{bmatrix} A_{11}^1 & A_{11}^2 & \dots & A_{11}^{D_O} \\ A_{22}^1 & A_{22}^2 & \dots & A_{22}^{D_O} \\ \vdots & \vdots & \ddots & \vdots \\ \vdots & \vdots & \ddots & \vdots \\ A_{ZZ}^1 & A_{ZZ}^2 & \dots & A_{ZZ}^{D_O} \end{bmatrix}, \quad (1)$$

and perform its singular value decomposition, $\mathcal{R} = \mathcal{U}\tilde{\Lambda}\mathcal{V}^T$. Here, \mathcal{U} and \mathcal{V} are orthogonal matrices of dimensions $Z \times Z$ and $D_O \times D_O$, respectively. Additionally, $\tilde{\Lambda} = \text{diag}[\tilde{\lambda}_1, \tilde{\lambda}_2, \dots, \tilde{\lambda}_{\min(D_O, Z)}]$, and its elements on the main diagonal are the so-called singular

values, while all other elements vanish. The rank of \mathcal{R} is at most $\min(D_O, Z)$, and in practice $D_O < Z$. Numerically, we always perform the so-called thin SVD instead of the full SVD, in which only the first D_O columns of the matrix \mathcal{U} are retained, while $\tilde{\Lambda}$ becomes a square matrix of dimension $D_O \times D_O$. The compression of \mathcal{R} consists of finding a matrix $\tilde{\mathcal{R}}$ with a smaller rank that is as close as possible to \mathcal{R} (formally, that minimizes $\|\mathcal{R} - \tilde{\mathcal{R}}\|$). According to the Eckart–Young–Mirsky theorem, this compression amounts to preserving the largest singular values and discarding the others. The number of preserved singular values sets the rank of $\tilde{\mathcal{R}}$. It can also be demonstrated [55], that the largest possible singular values, $\tilde{\lambda}_\alpha = \sqrt{Z}$, correspond to LIOMs, Q^α . These can be expressed in terms of the local operators introduced in Eq. (1), i.e., $Q^\alpha = \sum_{s=1}^{D_O} \mathcal{V}_{s\alpha} A^s$. In other words, the compression carried out for the initial set of operators $\{A^1, \dots, A^{D_O}\}$ finds all LIOMs that can be written as linear combinations of these operators.

In this work, we show that the LIOMs can be accurately estimated by compressing a small number of randomly selected rows of \mathcal{R} . While restricting the compression to a subset of eigenstates does not guarantee finding the true LIOMs, the problem remains well-posed, as it does not rely on the HS product. Specifically, we randomly select N_S eigenstates of the Hamiltonian that correspond to N_S rows of the matrix \mathcal{R} . These rows are then stored in the matrix R , for which we perform the singular value decomposition:

$$R = \begin{bmatrix} A_{11}^1 & \dots & A_{11}^{D_O} \\ \vdots & \ddots & \vdots \\ \vdots & \ddots & \vdots \\ A_{N_S N_S}^1 & \dots & A_{N_S N_S}^{D_O} \end{bmatrix} = U \text{diag}[\lambda_1, \lambda_2, \dots] V^T. \quad (2)$$

Next, we define the approximate LIOMs as

$$Q^\alpha = \sum_{s=1}^{D_O} \mathcal{V}_{s\alpha} A^s, \quad (3)$$

for the largest singular values λ_α . Moreover, we demonstrate that these approximate LIOMs are very close to the true LIOMs, $Q^\alpha \simeq \hat{Q}^\alpha$, for an unexpectedly small number of eigenstates, $N_S \ll Z$. We emphasize that, from now on, calligraphic letters denote quantities obtained from the full set of eigenstates, e.g., \mathcal{R} , while non-calligraphic letters denote corresponding quantities obtained from a subset of eigenstates, e.g., R .

The selected eigenstates are numerically obtained using the shift-invert method for the target energy E_T [64]. Since we focus on the translationally-invariant spin chains that conserve the total spin projection, we randomly choose N_S values of E_T , distributed across all considered magnetization and momentum sectors according to the appropriate binomial and uniform distributions, respectively. In each symmetry sector, the target energies are sampled with the probability density equal to

the many-body density of states, $\rho(E_T) = \frac{1}{Z} \sum_n \delta(E_T - E_n) = \exp[-E_T^2/(2L\sigma^2)]/\sqrt{2\pi L\sigma^2}$, which variance is obtained from the exact diagonalization of small systems with $L \in \{14, 16, 18, 20\}$. In this way, each eigenstate $|n\rangle$ has equal probability of being selected.

III. COMPRESSION-BASED APPROACH IN XXZ MODEL

As mentioned above, we consider the translationally-invariant spin models that preserve the total spin projection, $S_{tot}^z = \sum_l S_l^z$, where S_l are spin $s = \frac{1}{2}$ operators acting on site l . For this reason, we study operators that are also translationally-invariant, Hermitian, and commute with S_{tot}^z . We group these operators according to their support, M , i.e., the maximal number of consecutive sites on which they act nontrivially. For example, $\sum_l S_l^z S_{l+1}^z$ and $\sum_l S_l^+ S_{l+1}^z S_{l+2}^- S_{l+3}^- + \text{H.c.}$ both belong to a group with $M = 4$, whereas the former one also belongs to a group with $M = 2$.

We first establish the number of eigenstates required for finding LIOMs in the XXZ chain:

$$H = \frac{1}{2} \sum_l (S_l^+ S_{l+1}^- + S_l^- S_{l+1}^+) + \Delta \sum_l S_l^z S_{l+1}^z, \quad (4)$$

with $\Delta = 3/4$ used in all calculations. We consider two orthogonal sectors of operators constructed as

$$A_R = O + O^\dagger, \quad (5)$$

$$A_I = i(O - O^\dagger), \quad (6)$$

which for brevity will be referred to as *real* and *imaginary* operators, respectively.

Here, O are Pauli strings constructed from products of operators acting on individual sites. At each site l , we consider the set $\{S_l^+, S_l^-, S_l^z, I_l\}$, where I_l is identity operator acting on site l . From all possible operators O , we retain only these that commute with S_{tot}^z . The resulting operators A_R and A_I are made traceless and orthonormal.

It is worth noting that the XXZ chain hosts degeneracies. Two degenerate eigenstates either belong to different momentum sectors or both belong to the $k = 0$ or $k = \pi$ momentum sectors. Since the considered operators, A_R and A_I , are translationally invariant, they have no matrix elements between eigenstates from different momentum sectors. For this reason, we exclude the $k = 0$ and $k = \pi$ momentum sectors from our numerical simulations.

Nevertheless, it is possible to handle degeneracies (if not massive). To this end, the shift-invert procedure for each target energy, E_T , has to be run multiple times. Since we start from a new random state in each run, if the closest eigenvalue to E_T is degenerate, the procedure will converge to random non-orthogonal states from the degenerate subspace. On these states, we perform the SVD,

and obtain the dimension of the degenerate subspace and its orthogonal basis. This allows to correctly compute all matrix elements in this degenerate subspace, and include them in the R matrix, as explained in Ref. [55].

Using the algorithm described above, we have verified that consistent results are obtained if the $k = 0$ and $k = \pi$ momentum sectors are taken into account (not shown). Moreover, the problem of massive degeneracies is addressed in the section devoted to the fragmented systems, i.e., Sec. IV.

A. Local integrals of motion

We start with a compression problem for imaginary operators supported on up to $M = 4$ sites that are even under the spin-flip transformation $S_l^\pm \rightarrow S_l^\mp$ and $S_l^z \rightarrow -S_l^z$. This sector contains $D_O = 9$ operators, which permits the construction of only a single LIOM that corresponds to the energy current [65, 66],

$$Q^1 = \sum_{s=1}^3 \mathcal{V}_{s1} A^s, \quad (7)$$

where

$$A^1 = i \sum_l S_l^+ S_{l+1}^z S_{l+2}^- + \text{H.c.}, \quad (8)$$

$$A^2 = i \sum_l S_l^z S_{l+1}^- S_{l+2}^+ + \text{H.c.}, \quad (9)$$

$$A^3 = i \sum_l S_l^- S_{l+1}^+ S_{l+2}^z + \text{H.c.}, \quad (10)$$

while $\mathcal{V}_{11} \simeq 0.6860$ and $\mathcal{V}_{21} = \mathcal{V}_{31} \simeq 0.5145$, related by $\mathcal{V}_{21}/\mathcal{V}_{11} = \mathcal{V}_{31}/\mathcal{V}_{11} = \Delta$.

Figures 1(a)-1(c) show the average projection $\langle |V_{s1}| \rangle$, as defined in Eq. (3), which corresponds to the largest singular value λ_1 of the matrix R , see Eq. (2). The averaging is performed over different choices of N_S eigenstates of the Hamiltonian. We note that the overall sign of LIOMs (Q^α versus $-Q^\alpha$) is arbitrary and emerges randomly in the numerical procedure. For this reason, the averaging is carried out over the absolute values. The continuous lines in panels (a) and (b) show the average values $\langle |V_{11}| \rangle$ and $\langle |V_{21}| \rangle = \langle |V_{31}| \rangle$, respectively. The shaded areas indicate the corresponding standard deviations obtained for the smallest ($L = 14$) and largest ($L = 24$) systems, using consistent color coding. The edge of the former is marked with a thin black curve for visibility.

It is apparent that the the energy current (LIOM from Eq. (7)) can be accurately estimated already from $N_S = N^* \simeq 10 \div 10^2$ eigenstates. The average projections, $\langle |V_{11}| \rangle$ and $\langle |V_{21}| \rangle = \langle |V_{31}| \rangle$, become very close to the exact results, \mathcal{V}_{11} and $\mathcal{V}_{21} = \mathcal{V}_{31}$. The latter are marked with dashed lines in Figs. 1(a)-1(b). At the same time, the average projections on other operators, $\langle |V_{s1}| \rangle$ with $s \geq 4$, decrease as $1/\sqrt{N_S}$, see Fig. 1(c). This is accompanied by the rescaled singular value, $\langle \lambda_1^2 \rangle / N_S$, saturating to one for $N_S = N^*$, see Fig. 1(d). Not only

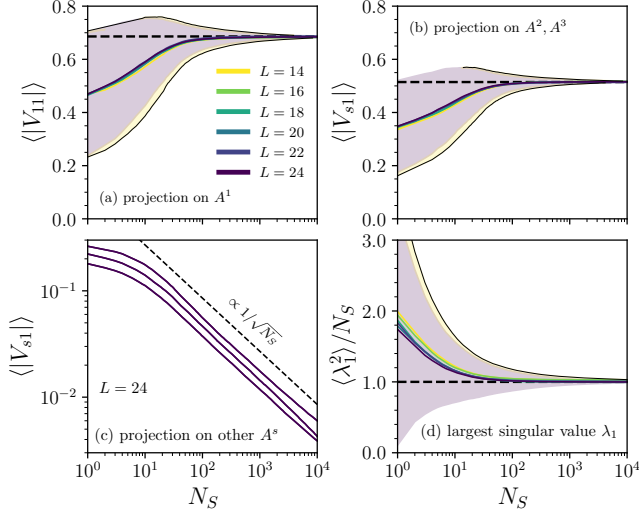


Figure 1. Numerical results for the largest singular value obtained for the set of imaginary operators that are even under the spin-flip transformation and supported on up to $M = 4$ sites. This set $\{A^1, \dots, A^{D_O}\}$ contains $D_O = 9$ operators including those in Eqs. (8)-(10). Continuous lines in (a) show the projection $\langle |V_{11}| \rangle$ averaged over different choices of N_S eigenstates for $L = 14, \dots, 24$. The number of these choices is 10^4 , also in Figs. 2-4. The shaded areas indicate the standard deviation of $|V_{11}|$ for the smallest ($L = 14$) and largest ($L = 24$) systems, using consistent color coding. The edge of the former is marked with a thin black curve for visibility. Additionally, the horizontal dashed line marks the analytical prediction, \mathcal{V}_{11} , for the energy current, \mathcal{Q}_1 , see Eq. (7). (b) The same results as in (a), but for the projection V_{21} . The projection V_{31} is indistinguishable from V_{21} on the presented scale. (c) Continuous lines show the projections $\langle |V_{s1}| \rangle$ on other operators ($s \geq 4$) for $L = 24$. (d) The largest singular value, $\langle \lambda_1^2 \rangle / N_S$, see Eq. (2). Strict LIOMs correspond to $\lambda^2/Z = 1$ obtained from all eigenstates (when $N_S = Z$).

do the average projections converge to the exact results, but their standard deviations also become very small. This implies that a randomly selected set of $N_S > N^*$ eigenstates allows to reconstruct the LIOM. Interestingly, the number of eigenstates needed for this purpose is almost independent of the system size or even slowly decreases with increasing L . The same finite-size scaling is observed for the standard deviations. Simultaneously, the dimension of the Hilbert space is exponential in L . Therefore, we can conclude that LIOMs can be obtained from an exponentially small fraction of eigenstates (e.g., $N_S = 100$ for $L = 24$ corresponds to only $\sim 10^{-5}$ of all eigenstates).

In order to explain what determines the minimal number of eigenstates, N^* , we have repeated the same calculations as in Fig. 1 but for a much larger set of local operators. To this end, we have expanded the support from $M = 4$ to $M = 6$, so that the compression problem is performed for the set of $D_O = 155$ operators. This set allows to reconstruct two LIOMs: the previously dis-

cussed \mathcal{Q}^1 and an additional \mathcal{Q}^2 corresponding to the second largest singular value λ_2 . The latter can be written as $\mathcal{Q}^2 = \sum_{s=1}^{21} \mathcal{V}_{s2} A^s$, where the two projections with largest magnitude are on

$$A^1 = i \sum_l S_l^+ S_{l+1}^z S_{l+2}^z S_{l+3}^z S_{l+4}^- + \text{H.c.}, \quad (11)$$

$$A^2 = i \sum_l S_l^z S_{l+1}^+ S_{l+2}^z S_{l+3}^z S_{l+4}^- + \text{H.c.}, \quad (12)$$

$$A^3 = i \sum_l S_l^+ S_{l+1}^- S_{l+2}^+ S_{l+3}^z S_{l+4}^- + \text{H.c.}, \quad (13)$$

$$A^4 = i \sum_l S_l^- S_{l+1}^+ S_{l+2}^+ S_{l+3}^z S_{l+4}^- + \text{H.c.}, \quad (14)$$

$$A^5 = i \sum_l S_l^+ S_{l+1}^z S_{l+2}^- S_{l+3}^+ S_{l+4}^- + \text{H.c.}, \quad (15)$$

$$A^6 = i \sum_l S_l^- S_{l+1}^z S_{l+2}^+ S_{l+3}^+ S_{l+4}^- + \text{H.c.}, \quad (16)$$

$$A^7 = i \sum_l S_l^+ S_{l+1}^z S_{l+2}^z S_{l+3}^- S_{l+4}^z + \text{H.c.}, \quad (17)$$

$$A^8 = i \sum_l S_l^+ S_{l+2}^z S_{l+3}^- + \text{H.c.}, \quad (18)$$

$$A^9 = i \sum_l S_l^z S_{l+2}^+ S_{l+3}^- + \text{H.c.}, \quad (19)$$

$$A^{10} = i \sum_l S_l^+ S_{l+1}^z S_{l+3}^- + \text{H.c.}, \quad (20)$$

$$A^{11} = i \sum_l S_l^+ S_{l+1}^- S_{l+3}^2 + \text{H.c.}, \quad (21)$$

with values $\mathcal{V}_{12} \simeq 0.3344$, $\mathcal{V}_{22} = \mathcal{V}_{42} = \mathcal{V}_{72} = \mathcal{V}_{82} = \mathcal{V}_{10,2} \simeq -0.2508$ and $\mathcal{V}_{32} = \mathcal{V}_{52} = \mathcal{V}_{62} = \mathcal{V}_{92} = \mathcal{V}_{11,2} \simeq 0.2508$.

The presence of more than one LIOM introduces a minor technical complication, making it difficult to compare the numerical results with the known analytical formulas. Note that an arbitrary rotation of two orthonormal LIOMs for $M = 6$, \mathcal{Q}_M^1 and \mathcal{Q}_M^2 , generates another pair of orthonormal LIOMs, \mathcal{Q}'_M^1 and \mathcal{Q}'_M^2 . They are related by $\mathcal{Q}_M^1 = \cos(\phi) \mathcal{Q}'_M^1 + \sin(\phi) \mathcal{Q}'_M^2$ and $\mathcal{Q}_M^2 = \cos(\phi) \mathcal{Q}'_M^2 - \sin(\phi) \mathcal{Q}'_M^1$. The singular value decomposition gives an arbitrarily rotated pair of LIOMs, \mathcal{Q}'_M^1 and \mathcal{Q}'_M^2 . The latter operators are also valid LIOMs, as they commute with the Hamiltonian and give the same contribution to the Mazur bound for any observable O , i.e., $\sum_{i=1}^2 \langle O \mathcal{Q}'_M^i \rangle^2 = \sum_{i=1}^2 \langle O \mathcal{Q}_M^i \rangle^2$, which provides a lower bound for the autocorrelation function of O [65, 67, 68]. Nevertheless, in known analytical formulas it is always assumed that $\mathcal{Q}_M^1 = \mathcal{Q}_{M-2}^1$, and so it is convenient to rotate the LIOMs obtained for a larger support such that they match the LIOMs obtained for a smaller M . Formally, this amounts to maximizing $\langle \mathcal{Q}_M^1 \mathcal{Q}_{M-2}^1 \rangle^2$, which is achieved for the rotation angle satisfying

$$\tan(2\phi) = \frac{2\langle \mathcal{Q}'_M^1 \mathcal{Q}_{M-2}^1 \rangle \langle \mathcal{Q}'_M^2 \mathcal{Q}_{M-2}^1 \rangle}{\langle \mathcal{Q}'_M^1 \mathcal{Q}_{M-2}^1 \rangle^2 - \langle \mathcal{Q}'_M^2 \mathcal{Q}_{M-2}^1 \rangle^2}. \quad (22)$$

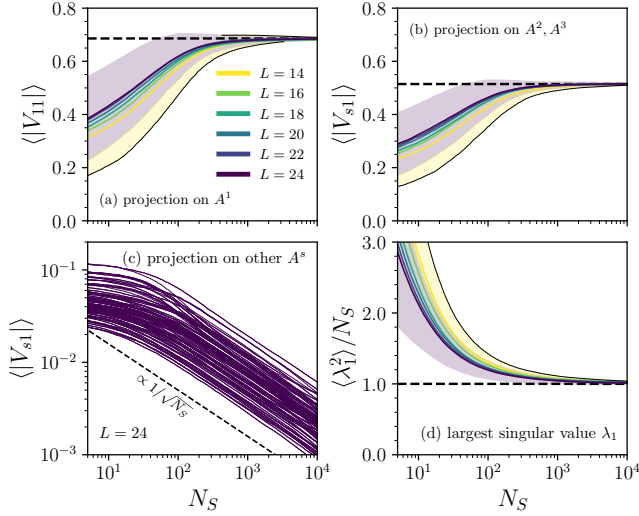


Figure 2. The same as in Fig. 1, but for a larger support $M = 6$, for which the set $\{A^1, \dots, A^{D_O}\}$ contains $D_O = 155$ operators. The approximate LIOMs corresponding to two largest singular values, Q^1 and Q^2 , are rotated according to the procedure described in the main text, see Eq. (22). (a) and (b) show the projections of Q^1 on the operators from Eqs. (8) and (9), respectively. The projections on operators from Eqs. (9)-(10) are mutually indistinguishable on the presented scale. (c) The projections of Q^1 on other operators with $s \geq 4$. Dashed lines in (a) and (b) mark the analytical predictions, as explained below Eq. (10).

The same rotation can be performed for the approximate LIOMs from Eq. (3). Namely, for each set of N_S eigenstates, we have determined Q_{M-2}^1 as well as a pair Q_M^1 and Q_M^2 , which is then rotated according to the procedure described above. As a result, we have obtained two approximate LIOMs: $Q_M^1 \simeq Q_{M-2}^1$ and an additional Q_M^2 . Figures 2 and 3(a) show results for $Q^1 = Q_M^1$ and $Q^2 = Q_M^2$, respectively.

We observe that the conclusions drawn from Fig. 1 remain valid for larger supports ($M = 6$) and more complicated LIOMs (Q^2). However, the more operators are considered, the more eigenstates are needed. In other words, N^* increases with M . By comparing the numerical results for several M , we find that the estimation of LIOMs is effective when the ratio $N^*/\text{rank}(\mathcal{R})$ is of the order of $\mathcal{O}(1) \div \mathcal{O}(10)$. In Fig. 1, $M = 4$ and $\text{rank}(\mathcal{R}) = 5$, while in Fig. 2, $M = 6$ and $\text{rank}(\mathcal{R}) = 57$. The relation between N^* and $\text{rank}(\mathcal{R})$ is consistent with the fact that the LIOMs are obtained from a compression that reduces the rank of R . For $N_S < \text{rank}(\mathcal{R})$, the rank is limited by the number of eigenstates, N_S . The compression then determines which states are the most relevant for the information contained in the matrix R and need to be preserved while reducing its rank. Only for $N_S > \text{rank}(\mathcal{R})$ is the rank limited by the number of operators, D_O . In this case, the compression selects the most relevant operators, i.e., the LIOMs. Therefore, the

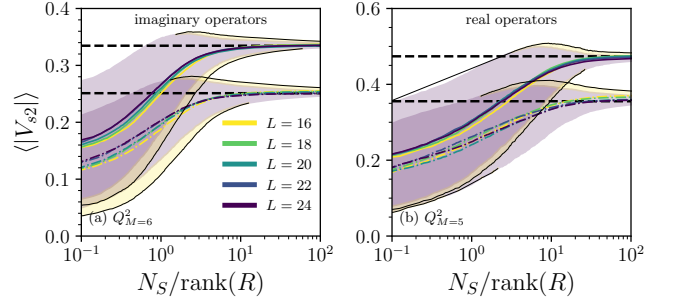


Figure 3. (a) The same as in Figs. 2(a) and 2(b) but for Q^2 instead of Q^1 . This panel shows the projections of Q^2 on the operators from Eqs. (11)-(21). The largest projection is on A^1 from Eq.(11), while the projections on other operators are mutually indistinguishable on the scale shown in (a). The horizontal dashed lines mark the analytical predictions, see text below Eq. (21). The number of eigenstates N^* is rescaled by $\text{rank}(\mathcal{R}) = 57$. (b) The numerical results for Q^2 constructed from the set of real operators that are even under the spin-flip transformation and are supported on up to $M = 5$ sites. In this sector, Q^1 represents the normalized Hamiltonian. This plot shows the projections of Q^2 on the operators from Eqs. (23)-(28). The largest projection is on A^1 from Eq. (23) and the projections on other operators are indistinguishable on the scale shown in (b). The number of eigenstates N^* is rescaled by $\text{rank}(\mathcal{R}) = 31$.

fact that $N^* > \text{rank}(\mathcal{R})$ is not very surprising. What is, however, surprising is that the estimation of LIOMs becomes effective very soon after exceeding the threshold $N^* = \text{rank}(\mathcal{R})$, i.e., soon after the compression starts to target operators instead of states.

Finally, we confirm that these findings hold in other symmetry sectors. Figure 3(b) shows results of an analogous study, but for the real operators that are even under the spin-flip transformation and are supported on up to $M = 5$ sites. This allows to reconstruct two LIOMs. Specifically, the Hamiltonian $Q^1 = H/\|H\|$ and an additional LIOM Q^2 , which can be written as $Q^2 = \sum_{s=1}^{10} \mathcal{V}_{s2} A^s$, where the projections with two largest magnitudes are on

$$A^1 = \sum_l S_l^+ S_{l+1}^z S_{l+2}^z S_{l+3}^- + \text{H.c.}, \quad (23)$$

$$A^2 = \sum_l S_l^+ S_{l+2}^- + \text{H.c.}, \quad (24)$$

$$A^3 = \sum_l S_l^+ S_{l+1}^z S_{l+2}^- S_{l+3}^z + \text{H.c.}, \quad (25)$$

$$A^4 = \sum_l S_l^- S_{l+1}^+ S_{l+2}^+ S_{l+3}^- + \text{H.c.}, \quad (26)$$

$$A^5 = \sum_l S_l^+ S_{l+1}^- S_{l+2}^+ S_{l+3}^- + \text{H.c.}, \quad (27)$$

$$A^6 = \sum_l S_l^z S_{l+1}^+ S_{l+2}^z S_{l+3}^- + \text{H.c.}, \quad (28)$$

with $\mathcal{V}_{12} \simeq 0.4739$, $\mathcal{V}_{22} = \mathcal{V}_{32} = \mathcal{V}_{42} = \mathcal{V}_{62} \simeq 0.3554$

and $\mathcal{V}_{52} \simeq -0.3554$. As before, the approximate LIOMs can be obtained via the rotation of Q_M^1 and Q_M^2 with respect to $Q_{M-2}^1 \simeq H/\|H\|$. Figure 3(b) show results for $Q^2 = Q_M^2$.

B. Quasiloal integrals of motion

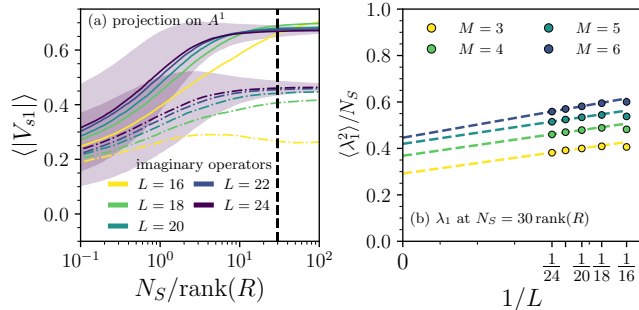


Figure 4. Results for the sector of imaginary operators that are odd under the spin-flip transformation. We consider the set of operators with the support $M = 6$, for which $\text{rank}(R) = 66$. This symmetry sector includes the spin-current operator but does not contain any LIOMs. (a) The projections of Q^1 onto the operators defined in Eqs. (29)-(30). The shaded areas indicate the standard deviations for the largest ($L = 24$) systems, using consistent color coding. (b) The largest singular value, $\langle \lambda_1^2 \rangle / N_s$, obtained for $N_s = 30 \text{rank}(R)$. The extrapolation to $L \rightarrow \infty$ indicates that it increases with increasing support in the thermodynamic limit, and suggest that it corresponds to a QLIOM.

We now verify whether the existence of quasiloal integrals of motion (QLIOMs) can also be established from a vanishing fraction of all eigenstates. Unlike LIOMs, which are strictly local, QLIOMs have exponentially small but nonzero weights on operators acting over arbitrarily large distances [30, 61, 69, 70]. Therefore, even when all eigenstates are taken into account (i.e., $N_s = Z$), QLIOMs cannot be reproduced exactly from the set of operators with an arbitrary finite support. This is reflected in the ratio λ^2/Z , which remains smaller than one for any finite M and approaches unity only in the limit $M \rightarrow \infty$. Despite this, a QLIOM can still contribute to the Mazur bounds for local operators, affecting their dynamics and even preventing their thermalization. The requirement, which can also be regarded as a criterion for quasilocality, is that its projection onto some of the operators with finite support, $\mathcal{V}_{s\alpha}$, remains nonzero in the thermodynamic limit.

In order to detect QLIOMs, we have studied the sector of imaginary operators that are odd under the spin-flip transformation. This sector contains, for example, the spin current operator. At the same time, it does not contain LIOMs, so that the largest singular values obtained from Eq. (2) may correspond to QLIOMs. Figure 4(a) shows results for the largest projections of Q^1 , which are

found for the following local operators:

$$A^1 = i \sum_l S_l^+ S_{l+1}^- + \text{H.c.}, \quad (29)$$

$$A^2 = i \sum_l S_l^+ S_{l+2}^- + \text{H.c.} \quad (30)$$

The numerical calculations were performed for the set $\{A^1, \dots, A^{D_O}\}$, which included operators with support on up to $M = 6$ sites.

Similarly to the cases discussed above, these projections, V_{s1} with $s \leq 2$, converge already for a small number of eigenstates, $N^* \simeq \text{rank}(\mathcal{R}) \div 10 \text{rank}(\mathcal{R})$. Since they do not decrease with L and $\lim_{L \rightarrow \infty} V_{s1} = \mathcal{V}_{s1}$, we expect that Q^1 is indeed a quasiloal operator. We also show how the corresponding singular value λ_1 depends on L and M in Fig. 4(b). These results have been obtained for $N_s/\text{rank}(R) = 30$, which is marked by the dashed vertical line in the panel (a). While we are not able to obtain the accurate value of $\lim_{M \rightarrow \infty} \lim_{L \rightarrow \infty} \langle \lambda_1^2 \rangle / N_s$, we observe that it is close to unity, as it should be for a conserved operator.

To conclude this section, we note that in the Bethe-ansatz integrable XXZ chain, LIOMs can be well estimated from just a tiny fraction of eigenstates. Moreover, the larger the system, the fewer eigenstates are needed. This holds true for all considered symmetry sectors as well as for the detection of quasiloal integrals of motions. We emphasize that for a fixed size, L , and support, M , taking into account more eigenstates does not yield any additional significant information regarding the existence or the structure of LIOMs or QLIOMs.

IV. COMPRESSION-BASED APPROACH IN FRAGMENTED SYSTEM

Hilbert-space fragmentation is an ergodicity-breaking phenomenon believed to be distinct from integrability [47–51]. However, many of the measures conventionally used to characterize closed quantum systems – such as spectral statistics [71–73], entanglement entropy [7–11], matrix elements of local observables [74–78] and fidelity susceptibilities [79–84] – exhibit very similar behavior in both cases. Consequently, it remains unclear whether, and if so, which properties fundamentally distinguish these two mechanisms of ergodicity breaking.

When written in a local basis (e.g., the computational basis), the Hamiltonian of a fragmented system shatters into exponentially many disconnected blocks. For the dimension of the largest block, Z_B , one requires that $\lim_{L \rightarrow \infty} Z_B/Z = 0$. Therefore, for a few randomly selected eigenstates, it is natural to expect that they all belong to different disconnected Krylov subspaces. To investigate whether this property affects the construction of LIOMs (whether it influences how information about the LIOMs is encoded in the eigenstates), we consider

the folded XXZ model [58–60]:

$$H = \sum_l \left(\frac{1}{4} + S_{l-1}^z S_{l+2}^z \right) (S_l^+ S_{l+1}^- + S_l^- S_{l+1}^+) + g \sum_l (S_l^z S_{l+2}^z + S_l^z S_{l+3}^z). \quad (31)$$

The spin-flip term in Eq. (31) conserves the number of domain walls,

$$A^1 = \sum_l S_l^z S_{l+1}^z. \quad (32)$$

Therefore, when $g = 0$, the Hamiltonian from Eq. (31) emerges as an effective model of the XXZ chain in the limit of infinite Δ , see Eq. (4). We have added an additional term $\sim g$ to be able to break the Bethe-ansatz integrability without destroying the fragmentation of the Hilbert space. This term allows us to determine the origin of the anomalous behavior that emerges from the numerical studies, as demonstrated below.

The folded XXZ model has massively degenerate eigenstates. For this reason, one needs to introduce a few technical modifications to the method. Since we study translationally-invariant operators, for which nonvanishing matrix elements exist only within the momentum sectors, we consider degeneracies only within such sectors. Since degeneracies are present in all of them, we also take into account the $k = 0$ and $k = \pi$ momentum sectors. The matrix \mathcal{R} from Eq. (1) as well as R from Eq. (2) should always contain all matrix elements from a degenerate subspace, i.e., these matrices should store (in columns) all $A_{nm}^s = \langle n | \hat{A}^s | m \rangle$ for $E_m = E_n$ [55]. In order to facilitate the numerical calculations for a massively degenerate eigenproblem, we use the exact denationalization instead of the shift-invert method. Finally, we note that a random drawing of a fixed number of eigenstates in the case of degeneracies is ambiguous. One would also seek to avoid a situation in which states belonging to degenerate subspaces are more likely to be included in the matrix R than non-degenerate states. Therefore, instead of drawing N_S eigenstates, we draw N_D degenerate subspaces. In order to maintain consistency with the previous discussion, all numerical results will be presented in terms of

$$\tilde{N}_s = N_D \bar{Z}_D, \quad (33)$$

where \bar{Z}_D is the average dimension of the degenerate subspaces calculated from all momentum sectors. We note that in the nondegenerate case, \tilde{N}_s is identical to the previously considered N_S . Moreover, when all degenerate subspaces are taken into account, one obtains $\tilde{N}_s = Z$.

We first apply the compression-based approach to a small set of operators, which are built only from S_l^z and I_l operators at each site, and supported on up to $M = 4$ sites. For clarity, the trivially conserved total magnetization, $\sum_l S_l^z$, is excluded from this set. It contains a LIOM, $\mathcal{Q}^1 = A^1$ from Eq. (32), which we aim to single

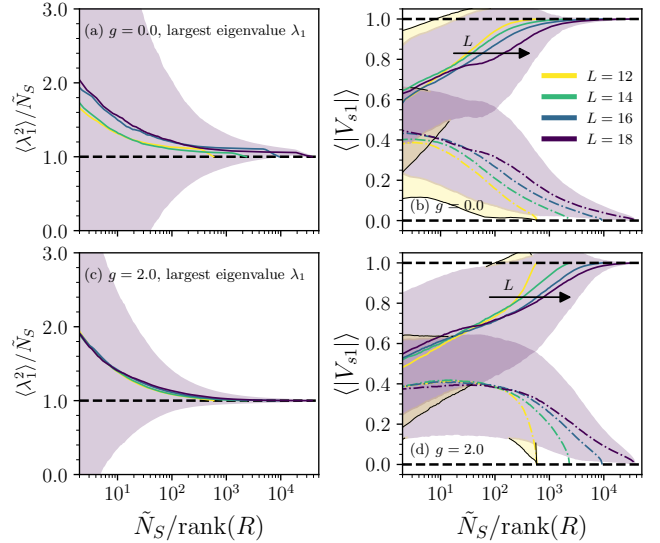


Figure 5. Results for the folded XXZ model from Eq. (31). The set of A^s is constructed only from S_l^z and I_l acting on up to $M = 4$ consecutive sites, for which $\text{rank}(R) = 7$. All results are averaged over 10^4 different choices of N_S eigenstates, also in Fig. 7. (a) The largest singular value, $\langle \lambda_1^2 \rangle / \tilde{N}_s$, for $g = 0$. (b) Top curves correspond to the largest projection of \mathcal{Q}^1 onto the operator A^1 from Eq. (32), while bottom curves correspond to the next largest projection. The shaded areas indicate the standard deviations of the projections for the smallest ($L = 12$) and largest ($L = 18$) systems, using consistent color coding. The edge of the former is marked with a thin black curve for visibility. Panels (c) and (d) show the same results as panels (a) and (b), respectively, but for the perturbed model with $g = 2.0$.

out for $g = 0$. Figure 5(a) shows the largest singular value, $\langle \lambda_1^2 \rangle / \tilde{N}_s$. Simultaneously, Fig. 5(b) demonstrates how the largest projection of \mathcal{Q}^1 onto $\mathcal{Q}^1 = A^1$ (continuous lines) and the second largest projection of \mathcal{Q}^1 (dashed lines) scales with \tilde{N}_s . As expected, $\langle \lambda_1^2 \rangle / \tilde{N}_s$ eventually approaches unity and the corresponding \mathcal{Q}^1 eventually becomes \mathcal{Q}^1 for large \tilde{N}_s . Nevertheless, in order to accurately estimate this LIOM, a majority of eigenstates has to be used ($N^* \simeq Z$), and the larger the system, the more eigenstates are required. This is exactly the opposite of the behavior observed earlier for the LIOMs in the XXZ model (with a finite Δ), cf. Fig. 2.

To unequivocally link \mathcal{Q}^1 with the Hilbert-space fragmentation, we have repeated the calculations while breaking the Bethe-ansatz integrability by setting $g = 2$. The corresponding results shown in Figs. 5(c) and 5(d) are very similar to the results for the integrable case shown in Figs. 5(a) and 5(b), respectively. This demonstrates that the conservation of \mathcal{Q}^1 is not related to the Bethe-ansatz integrability.

Interestingly, our numerical results indicate that \mathcal{Q}^1 is not the only conserved quantity arising from Hilbert space fragmentation and persisting for nonzero g . In Fig. 6, we present the second and third largest singu-

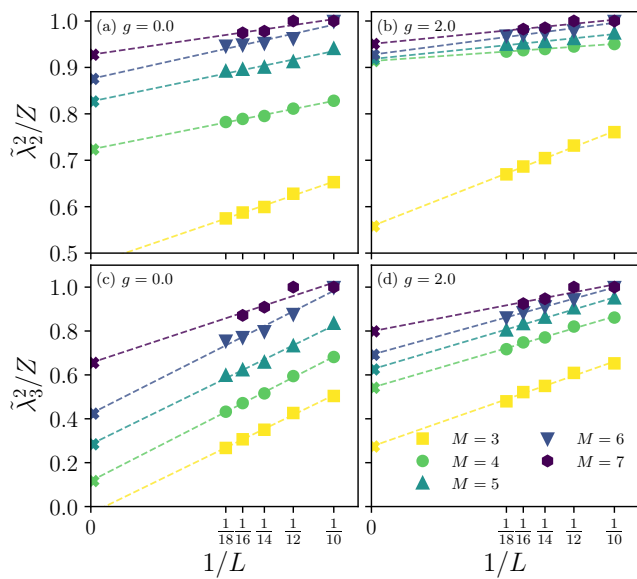


Figure 6. (a),(b) The second and (c),(d) third singular values in the folded XXZ model, which were obtained from the same set of operators as in Fig. 5 but for all eigenstates (i.e., $\tilde{N}_S = Z$). (a),(c) show the results for the unperturbed model with $g = 0.0$, while (b),(d) show the results for a relatively strong perturbation with $g = 2.0$.

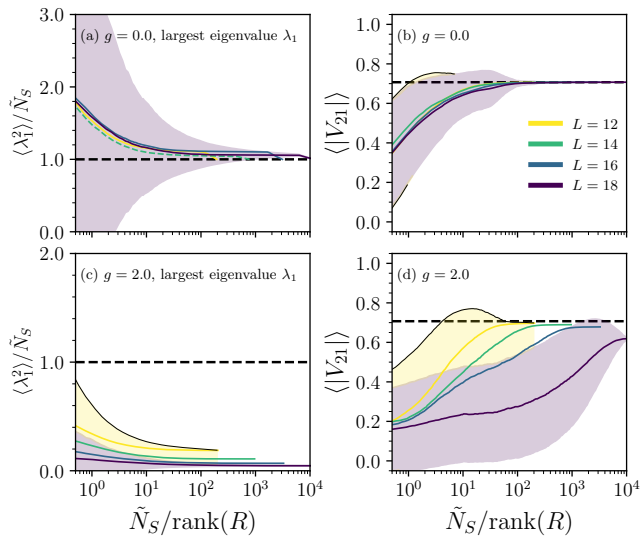


Figure 7. Results for the XXZ folded model, as in Fig. 5, but for another set of operators. Here, we have used the same set as in Fig. 1, for which $M = 4$ and $\text{rank}(R) = 5$. (b),(d) show the largest projection of Q^1 on the operator A^2 from Eq (9).

lar values obtained for the same set of operators, which are built only from products of S_l^z and I_l . In this particular case, we have used all eigenstates of the Hamiltonian from Eq. (31), i.e., $\tilde{N}_s = Z$. Figure 6 shows how these singular values depend the system size L and the support M . The presence of QLIOMs is even more clear than in

the previously discussed case, see Fig. 4(b). In particular, $\lim_{M \rightarrow \infty} \lim_{L \rightarrow \infty} \tilde{\lambda}_{2,3}^2/Z$ approaches unity even more clearly. This is especially evident for the perturbed system with $g = 2$ [see Fig. 6(b) and 6(d)], reinforcing the claim that these conservation laws do not originate from the Bethe-ansatz integrability. To determine the exact structure of these QLIOMs, additional calculations are required, which lie beyond the scope of the present work.

Finally, we consider another set of operators, which allows for the construction of LIOMs that originate from the Bethe-ansatz integrability. Specifically, we consider the same set of operators that has previously been used for the XXZ model with $\Delta = 3/4$, for which results are shown in Fig. 1. For the case of the folded XXZ model, the largest singular value, $\langle \lambda_1^2 \rangle / \tilde{N}_s$, is shown in Fig. 7(a). The corresponding Q^1 represents the energy current and its largest projection on the operator A^1 from Eq. (8) is plotted in Fig. 7(b). In order to connect the obtained integral of motion to the Bethe-ansatz integrability, we have repeated the same calculations but for $g = 2$, see Figs. 7(c) and 7(d). It is clear that when g is different from zero, the same set of operators does not contain any LIOM. The comparison of Figs. 7(a) and 7(b) with Figs. 1(d) and 1(a), respectively, shows that Hilbert-space fragmentation does not prevent the construction of LIOMs, provided that these LIOMs do not originate from it. Even in its presence, such LIOMs can be reliably estimated from $N^* \simeq \text{rank}(R) \div 10 \text{rank}(R)$ eigenstates.

Since the energy current can be reconstructed from a small number of eigenstates, $N^* \ll Z$, the inability to do the same for LIOMs originating from the Hilbert space fragmentation does not appear to be merely a consequence of massive degeneracies. One might expect that the information about LIOMs is not contained in individual eigenstates within a degenerate subspace, but is instead somehow distributed among them. In such a case, including a single degenerate subspace is more akin to including a single non-degenerate eigenstate. Note that for $L = 16$, when the Hilbert space dimension is 65536, there are 8314 (momentum-resolved) degenerate subspaces with an average dimension of 8, while the maximal dimension of 665. Yet, the observed inability appears to reflect a more subtle property of fragmented systems.

V. CONCLUDING REMARKS

In this work, we have demonstrated that integrability leaves a significant imprint on individual eigenstates, enabling the reconstruction of local integrals of motion (LIOMs) from an incomplete spectrum. This greatly broadens our understanding of the information encoded in individual eigenstates. Specifically, their small number not only allows the identification of ergodic systems and the estimation of their thermal properties, but also makes it possible to establish local conservation laws in integrable systems and, consequently, to estimate the properties of

their stationary states.

We construct LIOMs by compressing information contained in the diagonal (or, more generally, equal-energy) matrix elements of local observables. This compression problem is well defined even for an incomplete set of eigenstates. Studying the XXZ chain, which is integrable, we find that LIOMs can be constructed from a set of D_O local operators using a number of eigenstates only slightly larger than D_O . This number does not grow with the system size, and the variations across different choices of eigenstates remain small. These properties hold for LIOMs in different symmetry sectors as well as for quasilocal integrals of motion.

In contrast, the described properties are violated in the folded XXZ model, which exhibits the Hilbert-space fragmentation. The model exhibits conserved quantities that

are unrelated to Bethe-ansatz integrability, since they remain robust under perturbation that breaks integrability but preserves fragmentation. Interestingly, constructing these conserved quantities requires access to almost the entire set of eigenstates. We argue that this cannot be attributed solely to the massive degeneracies present in the model. This finding represents one of the few fundamental differences known between integrability and fragmentation.

ACKNOWLEDGMENTS

We acknowledge fruitful discussions with Lev Vidmar. This work was supported by the National Science Centre (NCN), Poland via project 2023/49/N/ST3/01033.

-
- [1] M. Rigol, V. Dunjko, and M. Olshanii, Thermalization and its mechanism for generic isolated quantum systems, *Nature* **452**, 854–858 (2008).
- [2] A. Polkovnikov, K. Sengupta, A. Silva, and M. Vengalattore, Nonequilibrium dynamics of closed interacting quantum systems, *Rev. Mod. Phys.* **83**, 863 (2011).
- [3] L. D’Alessio, Y. Kafri, A. Polkovnikov, and M. Rigol, From quantum chaos and eigenstate thermalization to statistical mechanics and thermodynamics, *Adv. Phys.* **65**, 239 (2016).
- [4] T. Mori, T. N. Ikeda, E. Kaminishi, and M. Ueda, Thermalization and prethermalization in isolated quantum systems: a theoretical overview, *J. Phys. B: At. Mol. Opt. Phys.* **51**, 112001 (2018).
- [5] J. R. Garrison and T. Grover, Does a single eigenstate encode the full Hamiltonian?, *Phys. Rev. X* **8**, 021026 (2018).
- [6] D. N. Page, Average entropy of a subsystem, *Phys. Rev. Lett.* **71**, 1291 (1993).
- [7] W. Beugeling, A. Andreanov, and M. Haque, Global characteristics of all eigenstates of local many-body Hamiltonians: participation ratio and entanglement entropy, *J. Stat. Mech.* **2015**, P02002 (2015).
- [8] L. Vidmar and M. Rigol, Entanglement entropy of eigenstates of quantum chaotic Hamiltonians, *Phys. Rev. Lett.* **119**, 220603 (2017).
- [9] M. Haque, P. A. McClarty, and I. M. Khaymovich, Entanglement of midspectrum eigenstates of chaotic many-body systems: Reasons for deviation from random ensembles, *Phys. Rev. E* **105**, 014109 (2022).
- [10] E. Bianchi, L. Hackl, M. Kieburg, M. Rigol, and L. Vidmar, Volume-law entanglement entropy of typical pure quantum states, *PRX Quantum* **3**, 030201 (2022).
- [11] M. Kliczkowski, R. Świątek, L. Vidmar, and M. Rigol, Average entanglement entropy of midspectrum eigenstates of quantum-chaotic interacting Hamiltonians, *Phys. Rev. E* **107**, 064119 (2023).
- [12] W. Buijsman, M. Haque, and I. M. Khaymovich, *Power-law banded random matrix ensemble as a model for quantum many-body Hamiltonians* (2025), [arXiv:2503.08825 \[cond-mat.dis-nn\]](https://arxiv.org/abs/2503.08825).
- [13] B. Bauer and C. Nayak, Area laws in a many-body localized state and its implications for topological order, *J. Stat. Mech.* **2013**, P09005 (2013).
- [14] M. Serbyn, Z. Papić, and D. A. Abanin, Local conservation laws and the structure of the many-body localized states, *Phys. Rev. Lett.* **111**, 127201 (2013).
- [15] K. Pawlik, P. Sierant, L. Vidmar, and J. Zakrzewski, Many-body mobility edge in quantum spin models, *Phys. Rev. B* **109**, L180201 (2024).
- [16] J. Suntajs, M. Hopjan, W. De Roeck, and L. Vidmar, Similarity between a many-body quantum avalanche model and the ultrametric random matrix model, *Phys. Rev. Res.* **6**, 023030 (2024).
- [17] P. Sierant, M. Lewenstein, A. Scardicchio, L. Vidmar, and J. Zakrzewski, Many-body localization in the age of classical computing, *Rep. Prog. Phys.* **88**, 026502 (2025).
- [18] M. Srednicki, The approach to thermal equilibrium in quantized chaotic systems, *J. Phys. A: Math. Theor.* **32**, 1163 (1999).
- [19] J. M. Deutsch, Eigenstate thermalization hypothesis, *Rep. Prog. Phys.* **81**, 082001 (2018).
- [20] R. Steinigeweg, A. Khodja, H. Niemeyer, C. Gogolin, and J. Gemmer, Pushing the limits of the eigenstate thermalization hypothesis towards mesoscopic quantum systems, *Phys. Rev. Lett.* **112**, 130403 (2014).
- [21] C. N. Yang and C. P. Yang, One-dimensional chain of anisotropic spin-spin interactions. I. Proof of Bethe’s hypothesis for ground state in a finite system, *Phys. Rev.* **150**, 321 (1966).
- [22] C. N. Yang and C. P. Yang, One-dimensional chain of anisotropic spin-spin interactions. II. Properties of the ground-state energy per lattice site for an infinite system, *Phys. Rev.* **150**, 327 (1966).
- [23] C. N. Yang and C. P. Yang, One-dimensional chain of anisotropic spin-spin interactions. III. Applications, *Phys. Rev.* **151**, 258 (1966).
- [24] W. Beugeling, R. Moessner, and M. Haque, Finite-size scaling of eigenstate thermalization, *Phys. Rev. E* **89**, 042112 (2014).
- [25] V. Alba, Eigenstate thermalization hypothesis and integrability in quantum spin chains, *Phys. Rev. B* **91**, 155123 (2015).
- [26] T. LeBlond, K. Mallayya, L. Vidmar, and M. Rigol, En-

- tanglement and matrix elements of observables in interacting integrable systems, *Phys. Rev. E* **100**, 062134 (2019).
- [27] M. Mierzejewski and L. Vidmar, Quantitative impact of integrals of motion on the eigenstate thermalization hypothesis, *Phys. Rev. Lett.* **124**, 040603 (2020).
- [28] M. Rigol, V. Dunjko, V. Yurovsky, and M. Olshanii, Relaxation in a completely integrable many-body quantum system: An ab initio study of the dynamics of the highly excited states of 1D lattice hard-core bosons, *Phys. Rev. Lett.* **98**, 050405 (2007).
- [29] B. Pozsgay, The generalized Gibbs ensemble for Heisenberg spin chains, *J. Stat. Mech.* **2013**, P07003 (2013).
- [30] E. Ilievski, J. De Nardis, B. Wouters, J.-S. Caux, F. H. L. Essler, and T. Prosen, Complete generalized Gibbs ensembles in an interacting theory, *Phys. Rev. Lett.* **115**, 157201 (2015).
- [31] L. Vidmar and M. Rigol, Generalized Gibbs ensemble in integrable lattice models, *J. Stat. Mech.* **2016**, 064007 (2016).
- [32] M. Kollar, F. A. Wolf, and M. Eckstein, Generalized Gibbs ensemble prediction of prethermalization plateaus and their relation to nonthermal steady states in integrable systems, *Phys. Rev. B* **84**, 054304 (2011).
- [33] A. C. Cassidy, C. W. Clark, and M. Rigol, Generalized thermalization in an integrable lattice system, *Phys. Rev. Lett.* **106**, 140405 (2011).
- [34] K. Fukai, Y. Nozawa, K. Kawahara, and T. N. Ikeda, Noncommutative generalized Gibbs ensemble in isolated integrable quantum systems, *Phys. Rev. Res.* **2**, 033403 (2020).
- [35] B. Bertini, M. Collura, J. De Nardis, and M. Fagotti, Transport in out-of-equilibrium XXZ chains: Exact profiles of charges and currents, *Phys. Rev. Lett.* **117**, 207201 (2016).
- [36] O. A. Castro-Alvaredo, B. Doyon, and T. Yoshimura, Emergent hydrodynamics in integrable quantum systems out of equilibrium, *Phys. Rev. X* **6**, 041065 (2016).
- [37] E. Ilievski and J. De Nardis, Microscopic Origin of Ideal Conductivity in Integrable Quantum Models, *Phys. Rev. Lett.* **119**, 020602 (2017).
- [38] B. Doyon and T. Yoshimura, A note on generalized hydrodynamics: Inhomogeneous fields and other concepts, *SciPost Phys.* **2**, 014 (2017).
- [39] S. Gopalakrishnan, D. A. Huse, V. Khemani, and R. Vasseur, Hydrodynamics of operator spreading and quasiparticle diffusion in interacting integrable systems, *Phys. Rev. B* **98**, 220303(R) (2018).
- [40] J. De Nardis, D. Bernard, and B. Doyon, Hydrodynamic diffusion in integrable systems, *Phys. Rev. Lett.* **121**, 160603 (2018).
- [41] U. Agrawal, S. Gopalakrishnan, R. Vasseur, and B. Ware, Anomalous low-frequency conductivity in easy-plane XXZ spin chains, *Phys. Rev. B* **101**, 224415 (2020).
- [42] A. J. Friedman, S. Gopalakrishnan, and R. Vasseur, Diffusive hydrodynamics from integrability breaking, *Phys. Rev. B* **101**, 180302 (2020).
- [43] A. Bastianello, A. D. Luca, and R. Vasseur, Hydrodynamics of weak integrability breaking, *J. Stat. Mech.* **2021**, 114003 (2021).
- [44] S. Gopalakrishnan and R. Vasseur, Anomalous transport from hot quasiparticles in interacting spin chains, *Rep. Prog. Phys.* **86**, 036502 (2023).
- [45] F. Hübner, E. Vernier, and L. Piroli, Generalized hydrodynamics of integrable quantum circuits, *SciPost Phys.* **18**, 135 (2025).
- [46] B. Doyon, S. Gopalakrishnan, F. Møller, J. Schmiedmayer, and R. Vasseur, Generalized hydrodynamics: A perspective, *Phys. Rev. X* **15**, 010501 (2025).
- [47] V. Khemani, M. Hermele, and R. Nandkishore, Localization from Hilbert space shattering: From theory to physical realizations, *Phys. Rev. B* **101**, 174204 (2020).
- [48] P. Sala, T. Rakovszky, R. Verresen, M. Knap, and F. Pollmann, Ergodicity-breaking arising from Hilbert space fragmentation in dipole-conserving Hamiltonians, *Phys. Rev. X* **10**, 011047 (2020).
- [49] S. Moudgalya, A. Prem, R. Nandkishore, N. Regnault, and B. A. Bernevig, Thermalization and its absence within Krylov subspaces of a constrained hamiltonian, in *Memorial Volume for Shoucheng Zhang* (World Scientific, 2021) p. 147–209.
- [50] S. Moudgalya, B. A. Bernevig, and N. Regnault, Quantum many-body scars and Hilbert-space fragmentation: A review of exact results, *Rep. Prog. Phys.* **85**, 086501 (2022).
- [51] G. Francica and L. Dell’Anna, Hilbert space fragmentation in a long-range system, *Phys. Rev. B* **108**, 045127 (2023).
- [52] P. Brighi, M. Ljubotina, and M. Serbyn, Hilbert space fragmentation and slow dynamics in particle-conserving quantum East models, *SciPost Phys.* **15**, 093 (2023).
- [53] S. Aditya, D. Dhar, and D. Sen, Subspace-restricted thermalization in a correlated-hopping model with strong hilbert space fragmentation characterized by irreducible strings, *Phys. Rev. B* **110**, 045418 (2024).
- [54] M. Ganguli, S. Aditya, and D. Sen, Aspects of Hilbert space fragmentation in the quantum east model: Fragmentation, subspace-restricted quantum scars, and effects of density-density interactions, *Phys. Rev. B* **111**, 045411 (2025).
- [55] P. Łydzba, P. Prelovšek, and M. Mierzejewski, Local integrals of motion in dipole-conserving models with Hilbert space fragmentation, *Phys. Rev. Lett.* **132**, 220405 (2024).
- [56] T. Rakovszky, P. Sala, R. Verresen, M. Knap, and F. Pollmann, Statistical localization: From strong fragmentation to strong edge modes, *Phys. Rev. B* **101** (2020).
- [57] S. Moudgalya and O. I. Motrunich, Hilbert space fragmentation and commutant algebras, *Phys. Rev. X* **12**, 011050 (2022).
- [58] B. Pozsgay, T. Gombor, A. Hutsalyuk, Y. Jiang, L. Pristyák, and E. Vernier, An integrable spin chain with Hilbert space fragmentation and solvable real time dynamics, *Phys. Rev. E* **104**, 044106 (2021).
- [59] L. Zadnik and M. Fagotti, The Folded Spin-1/2 XXZ Model : I. Diagonalization, Jamming, and Ground State Properties, *SciPost Phys. Core* **4**, 010 (2021).
- [60] L. Zadnik, K. Bidzhiev, and M. Fagotti, The folded spin-1/2 XXZ model: II. Thermodynamics and hydrodynamics with a minimal set of charges, *SciPost Physics* **10**, 1 (2021).
- [61] M. Mierzejewski, P. Prelovšek, and T. Prosen, Identifying local and quasilocal conserved quantities in integrable systems, *Phys. Rev. Lett.* **114**, 140601 (2015).
- [62] M. Mierzejewski, T. Prosen, and P. Prelovšek, Approximate conservation laws in perturbed integrable lattice models, *Phys. Rev. B* **92**, 195121 (2015).
- [63] M. Mierzejewski, M. Kozarzewski, and P. Prelovšek,

- Counting local integrals of motion in disordered spinless-fermion and Hubbard chains, *Phys. Rev. B* **97**, 064204 (2018).
- [64] F. Pietracaprina, N. Macé, D. J. Luitz, and F. Alet, Shift-invert diagonalization of large many-body localizing spin chains, *SciPost Physics* **5** (2018).
- [65] X. Zotos, F. Naef, and P. Prelovšek, Transport and conservation laws, *Phys. Rev. B* **55**, 11029 (1997).
- [66] M. Grabowski and P. Mathieu, Structure of the conservation laws in quantum integrable spin chains with short range interactions, *Ann. Phys.* **243**, 299–371 (1995).
- [67] P. Mazur, Non-ergodicity of phase functions in certain systems, *Physica* **43**, 533 (1969).
- [68] A. Dhar, A. Kundu, and K. Saito, Revisiting the Mazur bound and the Suzuki equality, *Chaos, Solitons and Fractals* **144**, 110618 (2021).
- [69] E. Ilievski, M. Medenjak, and T. Prosen, Quasilocal Conserved Operators in the Isotropic Heisenberg Spin-1/2 Chain, *Phys. Rev. Lett.* **115**, 120601 (2015).
- [70] T. Prosen and E. Ilievski, Families of quasilocal conservation laws and quantum spin transport, *Phys. Rev. Lett.* **111**, 057203 (2013).
- [71] V. Oganesyan and D. A. Huse, Localization of interacting fermions at high temperature, *Phys. Rev. B* **75**, 155111 (2007).
- [72] Y. Y. Atas, E. Bogomolny, O. Giraud, and G. Roux, Distribution of the ratio of consecutive level spacings in random matrix ensembles, *Phys. Rev. Lett.* **110**, 1 (2013).
- [73] P. Sierant and J. Zakrzewski, Level statistics across the many-body localization transition, *Phys. Rev. B* **99**, 104205 (2019).
- [74] D. Jansen, J. Stolpp, L. Vidmar, and F. Heidrich-Meisner, Eigenstate thermalization and quantum chaos in the Holstein polaron model, *Phys. Rev. B* **99** (2019).
- [75] C. Schönle, D. Jansen, F. Heidrich-Meisner, and L. Vidmar, Eigenstate thermalization hypothesis through the lens of autocorrelation functions, *Phys. Rev. B* **103**, 235137 (2021).
- [76] J. Richter, A. Dymarsky, R. Steinigeweg, and J. Gemmer, Eigenstate thermalization hypothesis beyond standard indicators: Emergence of random-matrix behavior at small frequencies, *Phys. Rev. E* **102**, 042127 (2020).
- [77] J. Wang, M. H. Lamann, J. Richter, R. Steinigeweg, A. Dymarsky, and J. Gemmer, Eigenstate thermalization hypothesis and its deviations from random-matrix theory beyond the thermalization time, *Phys. Rev. Lett.* **128**, 180601 (2022).
- [78] A. Dymarsky, Bound on eigenstate thermalization from transport, *Phys. Rev. Lett.* **128**, 190601 (2022).
- [79] M. Pandey, P. W. Claeys, D. K. Campbell, A. Polkovnikov, and D. Sels, Adiabatic eigenstate deformations as a sensitive probe for quantum chaos, *Phys. Rev. X* **10**, 041017 (2020).
- [80] D. Sels and A. Polkovnikov, Dynamical obstruction to localization in a disordered spin chain, *Phys. Rev. E* **104**, 054105 (2021).
- [81] T. LeBlond, D. Sels, A. Polkovnikov, and M. Rigol, Universality in the onset of quantum chaos in many-body systems, *Phys. Rev. B* **104**, L201117 (2021).
- [82] H. Kim and A. Polkovnikov, Integrability as an attractor of adiabatic flows, *Phys. Rev. B* **109**, 195162 (2024).
- [83] R. Świątek, P. Łydźba, and L. Vidmar, Fading ergodicity meets maximal chaos, *Phys. Rev. B* **111**, 184203 (2025).
- [84] M. Lisiecki, J. Bonča, M. Mierzejewski, J. Herbrych, and P. Łydźba, Tunable Hilbert space fragmentation and extended critical regime, *Phys. Rev. B* **112**, 195116 (2025).